Journal of Applied Sciences

ISSN 1812-5654

science alert

ANSInet
an open access publisher
http://ansinet.com

Journal of Applied Sciences 7 (10): 1351-1361, 2007
ISSN 1812-5654

Study of an Engineering Mixed Contact: Part II-Results for Isosceles Triangle Surface Ridges

Yongbin Zhang
Zhejiang Jinlei Electronic and Mechanical Co. Ltd.,
Zhejiang Province, Peoples's Republic of China

Abstracts: This research presents the results for isosceles triangle surface ridges obtained from the analysis. For the modeled contact, the load-carrying capacities and contact stiffness of different types of contact areas in the whole contact as well as of the whole contact are obtained for different surface ridge geometry parameter values. The contact pressure distributions, respectively in the conventional hydrodynamic lubricated area and the physical adsorbed boundary layer lubricated area in the present modeled contact are discussed. The temperature rises on the direct surface contact area in the present contact are also calculated for the selected operating conditions when the Poisson ratios, Young's moduli of elasticity and compressive yielding strengths of the contact surfaces are, respectively taken as insensitive to the contact surface temperature rise.

Key words: Engineering mixed contact, dry contact, oxidized chemical boundary layer, physical adsorbed boundary layer, hydrodynamic contact

INTRODUCTION

An analysis was presented by Zhang (2007) for an engineering mixed lubrication contact. In this contact, the whole contact was composed of three types of contact areas which are in different contact regimes. These contact areas are, respectively the direct surface contact area between the contact surface ridge and the smooth plane, the conventional hydrodynamic lubricated area in the contact where the lubricating film thickness is relatively high and the physical adsorbed boundary layer lubricated area in the contact where the film thickness is very low, the film is wholly physically adhering and ordering to the contact surfaces and the lubricating media is molecule and non-continuum across the film thickness; The direct surface contact area between the contact surfaces can be the oxidized chemical boundary layer contact area or the fresh metal-metal dry contact area. The contact regimes in the modeled contact were shown to be quite mixed. The modeled contact has a typical feature of and belongs to the future mode of mixed lubrication contact (Zhang, 2006a, b). It is believed to be more engineering and realistic. The present mode of contact is one of the modes of mixed lubrication contacts which requires to be studied. Results obtained for the present mode of contact are of significant interest.

In the analysis of this mode of contact (Zhang, 2007), two types of contact surface ridges were, respectively taken. They were isosceles triangle surface ridges and isosceles truncated triangle surface ridges. In treating the direct contact between the ridge and the smooth plane, the elastic-plastic contact problem was solved when this contact was loaded and deformed. In treating the conventional hydrodynamic lubricated area, the Reynolds equation was solved for finding the lubricating film pressure distribution and the lubricating film load-carrying capacity in this area. In solving the physical adsorbed boundary layer contact problem, the flow factor approach (Zhang and Lu, 2005; Zhang, 2006c, d) was used and the Reynolds equation was developed and solved to obtain the lubricating film pressure distribution and the lubricating film load-carrying capacity there. These analysis then gave the load-carrying capacity and contact stiffness of the whole contact.

The present study is the subsequent part of the study presented in the first part (Zhang, 2007). It presents the results obtained from the analysis presented in the first part (Zhang, 2007) when the contact surface ridge is taken as isosceles triangle. The performance of the present contact is obtained for this surface ridge.

CONTACT MODEL

For better understanding, the contact model and its ridge geometries studied in the present paper are shown in Fig. 1a. Figure 1b shows a picture of the studied contact under loading.

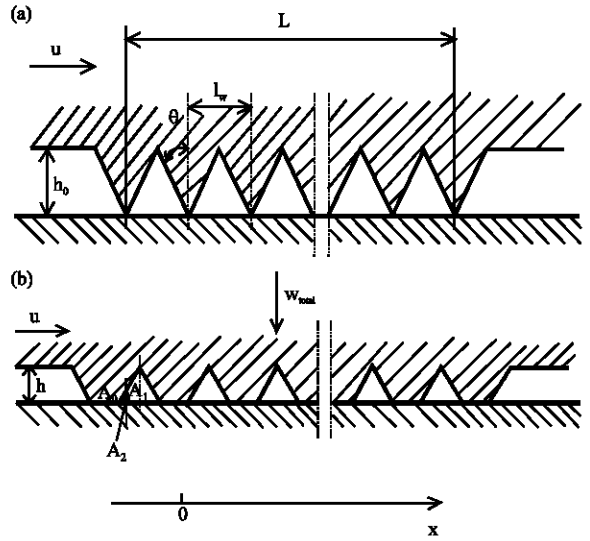

Fig. 1: Studied contact in the present study. (a) The contact model and its ridge geometries and (b) Picture of the contact under loading

OPERATIONAL PARAMETERS

The values of the operational parameters in the present study are chosen as follows:

h_0 = 1.6 μm,
p_y = 0.3 GPa,
E_a = 193 GPa,
v = 0.28,
α = 23.7GPa^{-1},
η_0 = 0.1 Pa.s,
u = (-) 30 m/s,
$h_{cr,ncf}$ = 30 nm,
f = 0.35,
k_m = 40 W/ (m.°C),
c_m = 400 J/(kg.°C),
ρ_m = 7800 kg /m^3,
N = 100

These operational parameters were shown in the first part (Zhang, 2007). The materials of the two contact surfaces are taken as same.

RESULTS

The results obtained from the analysis developed in the first part (Zhang, 2007) according to the above operational parameter values are demonstrated and discussed as follows when the contact surface ridge is isosceles triangle. The presented parameters in the results

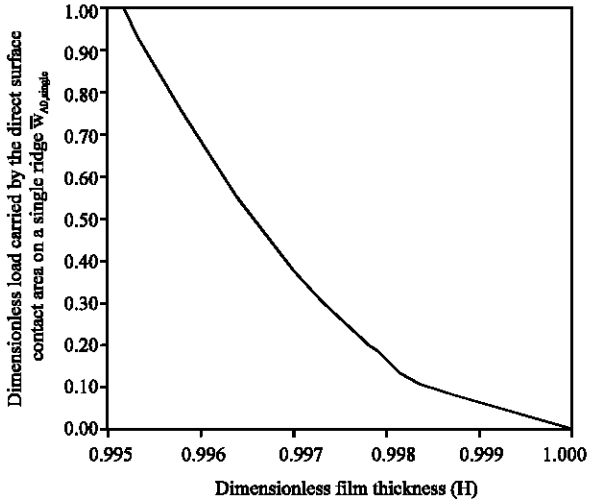

Fig. 2a: Variation of the load $\bar{w}_{A0,single}$ carried by the direct contact between a single ridge and the smooth plane with the dimensionless film thickness H when the half ridge angle θ is 25° and the ridge is in elastic deformation

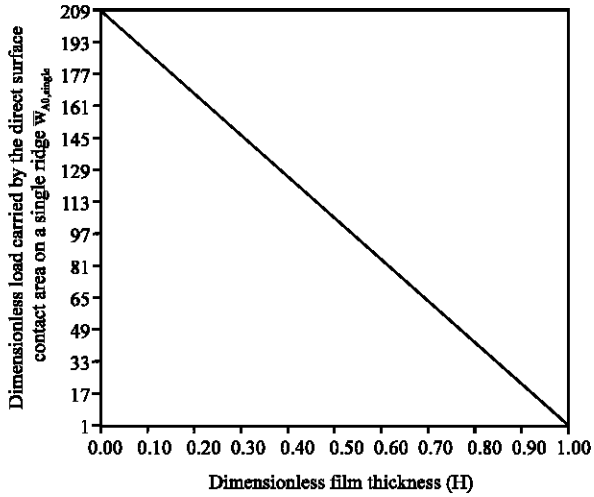

Fig. 2b: Variation of the load $\bar{w}_{A0,single}$ carried by the direct contact between a single ridge and the smooth plane with the dimensionless film thickness H when the half ridge angle θ is 25° and the ridge is in plastic deformation

are all in dimensionless form. The definitions of these dimensionless parameters are shown in the Nomenclature.

Load-carrying capacity, contact stiffness and critical elastic deformation of the direct contact between a single ridge and the smooth plane: Figure 2a shows the variation of the load $\bar{w}_{A0,single}$ carried by the direct contact between a single ridge and the smooth plane with the

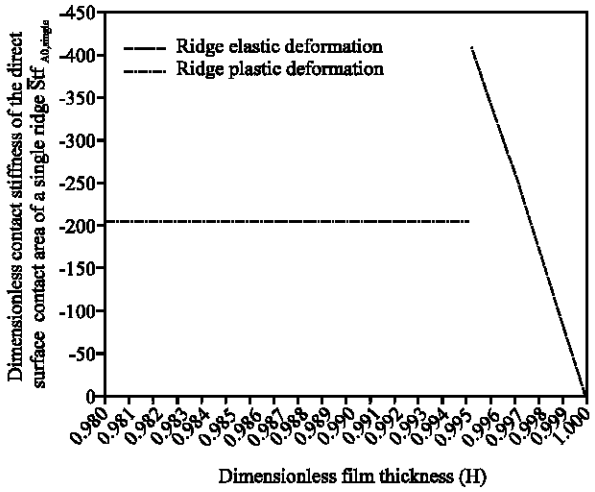

Fig. 3: Contact stiffness of the direct contact between a single ridge and the smooth plane covering the practical ridge deformations when the half ridge angle θ is 25°

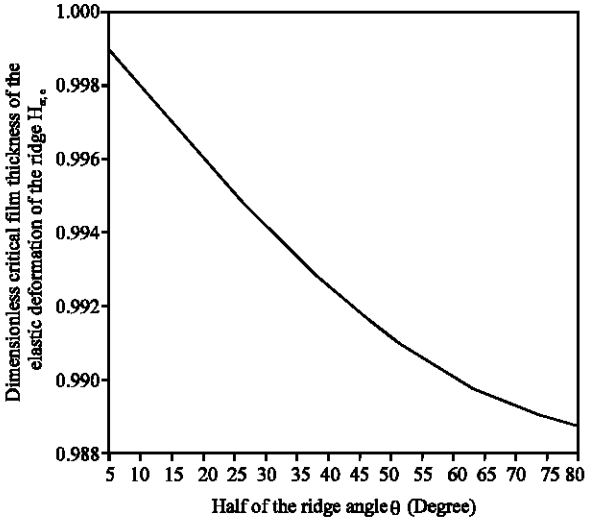

Fig. 4: Critical film thickness $H_{cr,e}$ in which the ridge reaches the maximum elastic deformation as function of the half ridge angle θ

dimensionless film thickness H when the half ridge angle θ is 25° and the ridge is in elastic deformation. It is shown that in the ridge elastic deformation regime the load $\overline{w}_{A0,single}$ is very sensitive to the variation of the film thickness H and drastically increased with the reduction of the film thickness H.

Figure 2b shows the variation of the load $\overline{w}_{A0,single}$ carried by the direct contact between a single ridge and the smooth plane with the dimensionless film thickness H when the half ridge angle θ is 25° and the ridge is in plastic deformation. It is shown that in the ridge plastic deformation regime the load $\overline{w}_{A0,single}$ is linearly increased with the reduction of the film thickness H.

Figure 3 shows the contact stiffness of the direct contact between a single ridge and the smooth plane covering the practical ridge deformations when the half ridge angle θ is 25°. It is shown that when the ridge is in elastic deformation, this contact stiffness is linearly and drastically increased with the reduction of the film thickness H; While, it is nearly half dropped when the ridge deformation transits from elastic to plastic and remains constant when the ridge is in plastic deformation.

Figure 4 shows the critical film thickness $H_{cr,e}$ in which the ridge reaches the maximum elastic deformation, as function of the half ridge angle θ. This critical film thickness is shown to reduce with the increase of the ridge angle θ. Since the critical interference for the ridge elastic deformation is equal to $(1-H_{cr,e})$, Fig. 4 shows that the increase of the ridge angle θ considerably increases the critical interference for the ridge elastic deformation and increases the ridge elasticity.

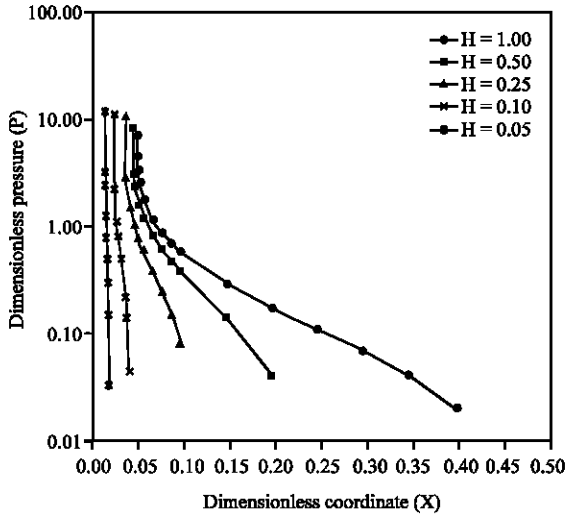

Fig. 5: Lubricant film pressure distributions in the conventional hydrodynamic lubricated area on a single ridge for different values of the film thickness H when the half ridge angle θ is 25°

Lubricant film pressure distribution, load-carrying capacity and contact stiffness of the conventional hydrodynamic lubricated area on a single ridge: Figure 5 shows the lubricant film pressure distributions in the conventional hydrodynamic lubricated area on a single ridge for different values of the film thickness H when the half ridge angle θ is 25°. It is shown that the hydrodynamic pressure zone (size in the X coordinate direction) is nearly equally proportionally reduced with the reduction of the film thickness H. When the film

thickness H is lower, this lubricant film pressure distribution is steeper. When the film thickness H is low, the conventional hydrodynamic lubricated area on a single ridge is shown to be narrow and the lubricant film pressure distribution in this area is very steep. However, when the film thickness H is high, this hydrodynamic lubricated area is fairly wide. The lubricant film pressure in this area is generally shown to be rapidly increased with the reduction of the coordinate X.

Figure 6 shows the carried loads $\bar{\bar{w}}_{Al,single}$ by the conventional hydrodynamic lubricated area on a single ridge as function of the film thickness H for different θ values. In computation of this load, the hydrodynamic pressure close to the physical adsorbed layer boundary lubrication area on a single ridge was neglected, since it is enormous and may cause significant contact surface deformations in its distributed area, these deformations may drop off this pressure to limited value and the contribution of this hydrodynamic pressure to the carried load by the whole conventional hydrodynamic lubricated area on a single ridge may be negligible due to its reduced value and narrow distribution area. For a given θ value, the load $\bar{\bar{w}}_{Al,single}$ is shown to be nearly linearly increased with the increase of the film thickness H. This increasing proportionality is greater for larger θ values. For small θ values, the value of the load $\bar{\bar{w}}_{Al,single}$ is small. For a given H value, the value of the load $\bar{\bar{w}}_{Al,single}$ is significantly increased with the increase of the half ridge angle θ. When the film thickness H is high and the half ridge angle θ is large, the value of the load $\bar{\bar{w}}_{Al,single}$ is quite large.

Figure 7 shows the contact stiffness $Stf_{Al,single}$ of the conventional hydrodynamic lubricated area on a single ridge for different values of the film thickness $\bar{H}$ and the half ridge angle θ. The contact stiffness $Stf_{Al,single}$ is significantly increased with the reduction of the film thickness H especially at low values of the film thickness H and large values of the half ridge angle θ. For a given value of the film thickness H, this contact stiffness is significantly increased with the increase of the half ridge angle θ.

Lubricant film pressure distributions in the physical adsorbed layer boundary lubrication area for different contact-lubricant interactions: In the investigation of the pressure generation in the physical adsorbed layer boundary lubrication area in the present contact, four types of the contact-lubricant interactions were used. They are, respectively named as strong interaction, medium interaction, weak interaction and no interaction and are, respectively represented by the values of the parameters a_i (i = 0, 1, 2) in the lubricant viscosity

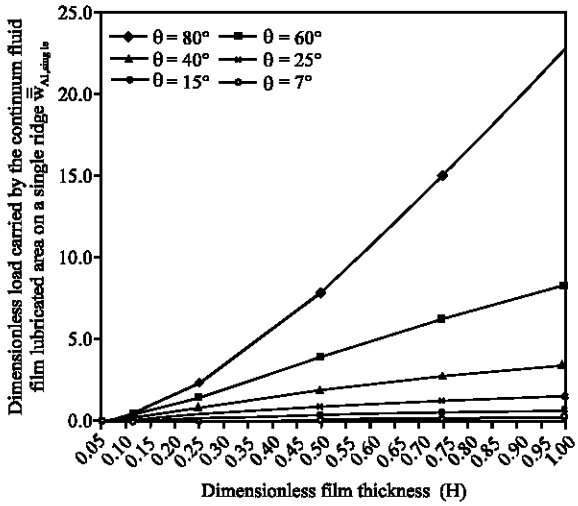

Fig. 6: Carried loads $\bar{\bar{w}}_{Al,single}$ by the conventional hydrodynamic lubricated area on a single ridge as function of the film thickness H for different θ values

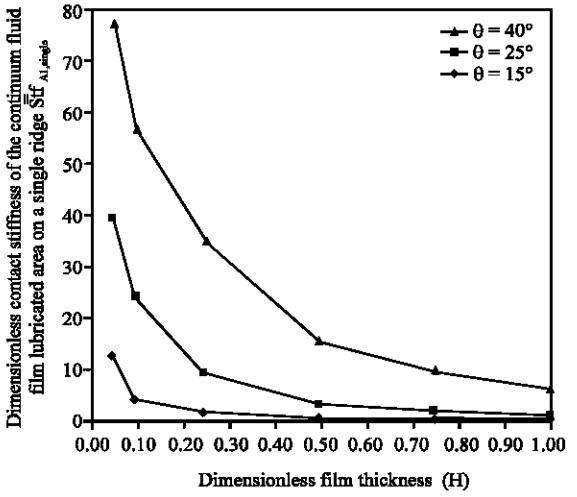

Fig. 7: Contact stiffness $\bar{Stf}_{Al,single}$ of the conventional hydrodynamic lubricated area on a single ridge for different values of the film thickness H and the half ridge angle θ

expression in this lubrication (Eq. 42) shown in the first part (Zhang, 2007). For better understanding, this lubricant viscosity expression is re-written as follows:

$$\eta_{ncf}^{eff} = \eta_0 e^{\alpha p} C_y(h_x) \qquad \text{for } r \le \frac{h_x}{h_{cr,ncf}} < 1 \qquad (1)$$

where

$$C_y(h_x) = a_0 + a_1(h_x / h_{cr,ncf})^{-1} + a_2(h_x / h_{cr,ncf})^{-2}$$

and r approaches zero.

The values of the parameters a_i (i = 0, 1, 2) appearing in Eq. 1 for the above four types of the contact-lubricant interactions are, respectively shown in Table 1.

The values of the parameter C_y in Eq. 1 for these four types of the contact-lubricant interactions are shown in Fig. 8, as function of the dimensionless film thickness $h_x/h_{cr,ncf}$. It is shown that when the contact-lubricant interaction exists, the value of the parameter C_y is increased with the reduction of the film thickness $h_x/h_{cr,ncf}$. This increase is particular significant at low values of the film thickness $h_x/h_{cr,ncf}$ and strong contact-lubricant interactions. The increase of the contact-lubricant interaction strength significantly increases the value of the parameter C_y especially at low values of the film thickness $h_x/h_{cr,ncf}$.

Figure 9 a and b, respectively show the lubricant film pressure distributions in the physical adsorbed layer boundary lubrication area on a single ridge for these four types of the contact-lubricant interactions when the dimensional film thickness h is 15 and 7.5 nm and the half ridge angle θ is 25°. It is shown that the lubricant film pressure is rapidly built up with the reduction of the coordinate X in this lubricated area. The stronger contact-lubricant interaction, the more rapid building-up of this pressure.

For a given X coordinate, the increase of the contact-lubricant interaction strength significantly increases the pressure in this lubricated area particularly when the X coordinate is away from the lubricant entrance of this lubricated area. When the film thickness h is lower, these effects are more significant.

Total load in the contact: Figure 10 a and b show the total loads carried, respectively by the whole contact, the conventional hydrodynamic lubricated areas and the direct surface contact areas between the contact surfaces in the present mixed lubrication, as function of the film thickness H when the contact surface ridge is, respectively in elastic and plastic deformations and the half ridge angle θ is 25°. In computation of the total load $\bar{w}_{total}$ carried by the whole contact, the load carried by the physical adsorbed layer boundary lubrication area in the present contact is neglected, since in the studied case this load may be negligible because of the very narrow zone occupied by the physical adsorbed layer boundary lubrication in the present contact and the actual considerably limited pressure in this lubricated area due to the contact surface deformations.

Table 1: Values of the parameters a_i (i=0, 1, 2) in Eq. 1 for the four types of the contact-lubricant interactions

	Parameter		
Interaction type	a_0	a_1	a_2
Strong interaction	1.8335	-1.4252	0.5917
Medium interaction	1.0822	-0.1758	0.0936
Weak interaction	0.9507	0.0492	1.6447E-4
No interaction	1.0	0.0	0.0

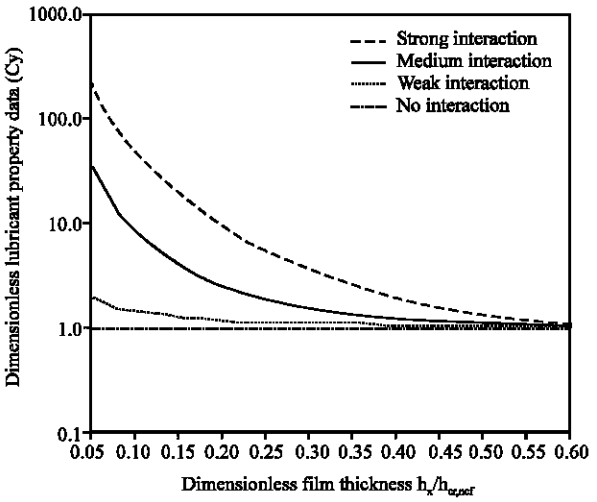

Fig. 8: Values of the parameter C_y in Eq. 1 for the four types of the contact-lubricant interactions as function of the dimensionless film thickness $h_x/h_{cr,ncf}$

It is shown by Fig. 10 a that in the present contact, when the contact surface ridge is in elastic deformation, with the reduction of the film thickness H, the total load carried by the direct contacts between the contact surfaces is rapidly increased, while the total load $\bar{w}_{A1\,total}$ carried by the conventional hydrodynamic lubricated areas nearly remains constant; In the present contact, the total load $\bar{w}_{total}$ carried by the whole contact is mainly contributed by the conventional hydrodynamic lubricated areas when the value of the film thickness H is between 0.997 and 1.0, while it is contributed by both the conventional hydrodynamic lubricated areas and the direct contacts between the contact surfaces in the ridge elastic deformation regime when the value of H is lower than 0.997. The total load $\bar{w}_{total}$ carried by the whole contact is shown to be rapidly increased with the reduction of the film thickness H when the contact surface ridge is in elastic deformation.

Figure 10b shows that in the present contact, when the contact surface ridge is in plastic deformation, the two total loads $\bar{w}_{total}$ and $\bar{w}_{A0.total}$ are linearly and rapidly increased with the reduction of the film thickness H, while

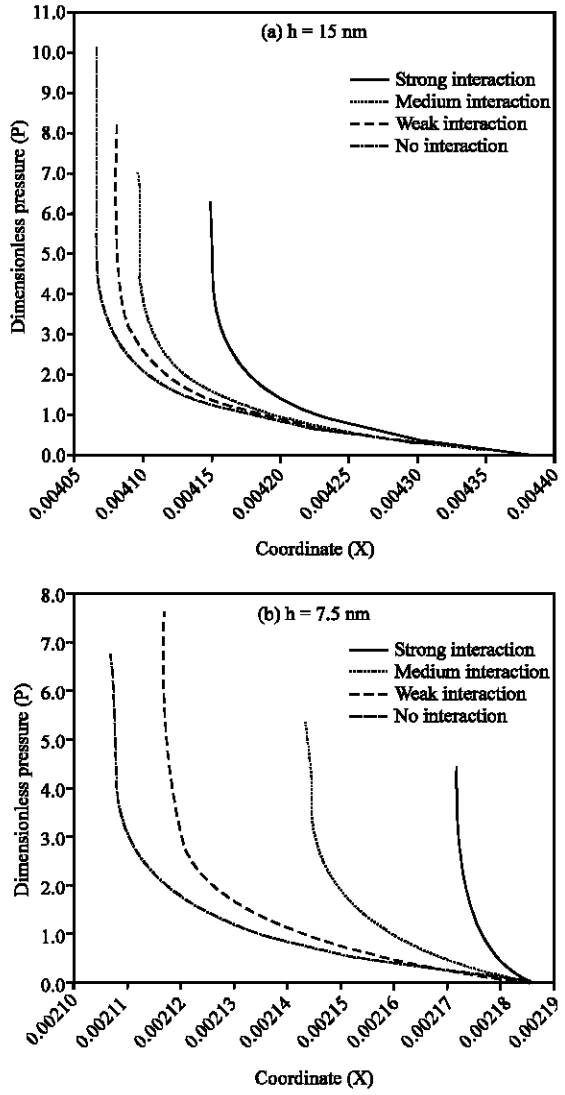

Fig. 9: Lubricant film pressure distributions in the physical adsorbed layer boundary lubrication area on a single ridge for the four types of the contact-lubricant interactions when the half ridge angle θ is 25°

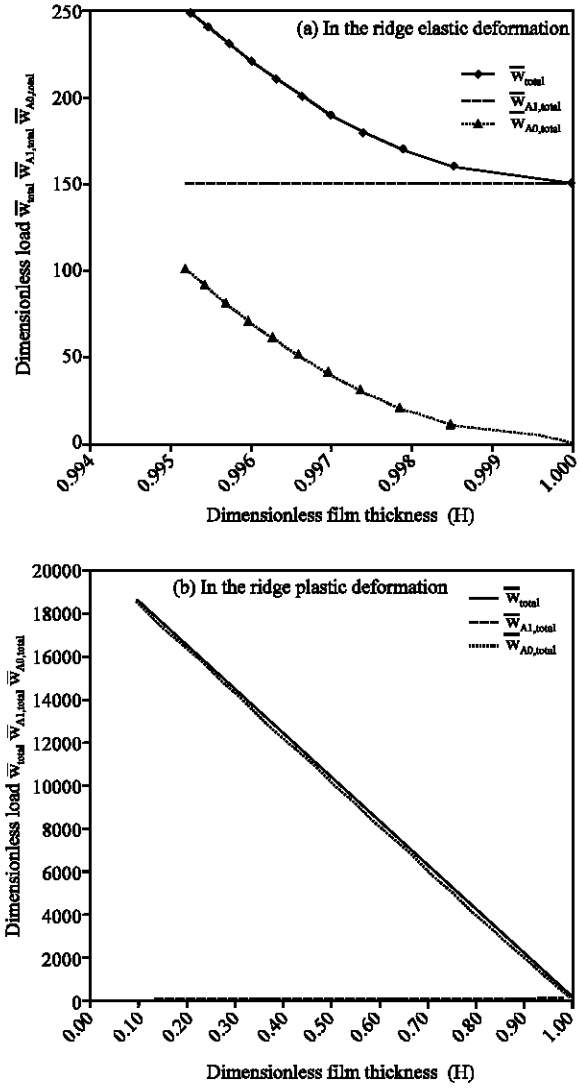

Fig. 10: Total loads carried, respectively by the whole contact, the conventional hydrodynamic lubricated areas and the direct surface contact areas between the contact surfaces in the present mixed lubrication as function of the film thickness H when the half ridge angle θ is 25°

the total load $\bar{w}_{A1,total}$ is linearly and gradually reduced with the reduction of the film thickness H. It is shown that in the ridge plastic deformation regime, the total load $\bar{w}_{total}$ carried by the whole contact is mainly contributed by the direct contacts between the contact surfaces, while the contribution of the conventional hydrodynamic lubricated areas to the total load carried by the whole contact is usually negligible. Figure 10b shows that when the load carried by the whole contact is heavy, it is mainly carried by the direct contacts between the contact surfaces and the performance of the present contact is determined by the performance of the direct contact between the contact surfaces.

Figure 11a and b show the loads $\bar{\bar{w}}_{ul,total}$ per unit contact width of the whole contact as function of the film thickness H for different values of the half ridge angle θ when the contact surface ridge deformations are, respectively elastic and plastic. Figure 11 a shows that for a given value of the half ridge angle θ, when the ridge is in elastic deformation, the value of the load $\bar{\bar{w}}_{ul,total}$ is

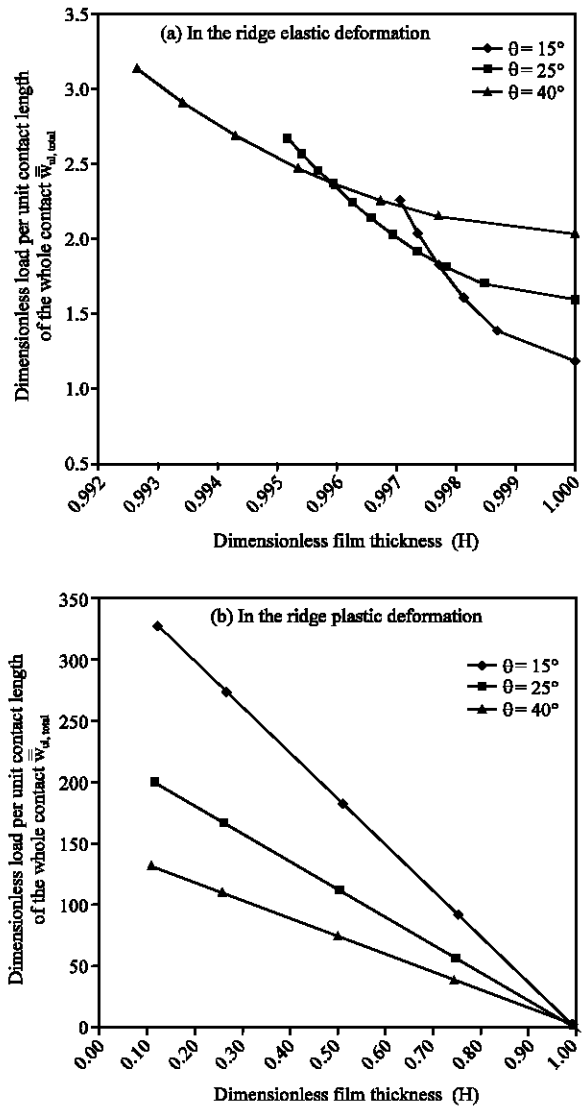

Fig. 11: The loads $\bar{\bar{w}}_{ul,total}$ per unit contact width of the whole contact as function of the film thickness H for different values of the half ridge angle θ

significantly increased with the reduction of the film thickness H particularly for smaller θ values; The larger value of the half ridge angle θ gives the larger load carried by the whole contact at the maximum ridge elastic deformation if the width of the whole contact is same. Figure 11a shows that when the ridge is in elastic deformation, a larger value of the half ridge angle θ tends to give a higher value of the load $\bar{\bar{w}}_{ul,total}$ and then a higher load-carrying capacity of the whole contact. This is due to the hydrodynamic lubrication effect between the contact surfaces. Figure 11b shows that for a given value of the half ridge angle θ, when the ridge is in plastic deformation, the value of the load $\bar{\bar{w}}_{ul,total}$ is linearly increased with the reduction of the film thickness H; This increasing proportionality is greater for smaller θ values. It is shown that when the ridge is in plastic deformation, a smaller value of the half ridge angle θ gives a higher value of the load $\bar{\bar{w}}_{ul,total}$ and then a higher load-carrying capacity of the whole contact. This is due to the direct contact effect between the contact surfaces.

Total contact stiffness: Figure 12a and b show the total contact stiffness of the whole contact, the conventional hydrodynamic lubricated areas and the direct contacts between the contact surfaces in the present contact as function of the film thickness H when the contact surface ridge is, respectively in elastic and plastic deformations and the half ridge angle θ is 25°.

Figure 12a shows that in the present contact, when the ridge is in elastic deformation, the total contact stiffness of the conventional hydrodynamic lubricated areas is positive and very small, while the magnitudes of the total contact stiffness of both the whole contact and the direct contacts between the contact surfaces are linearly rapidly increased with the reduction of the film thickness H. The contact stiffness of the whole contact is shown to be contributed mainly by the total contact stiffness of the direct contacts between the contact surfaces. It reaches large values even when the contact surface ridge is a little compressed.

Figure 12b shows that in the present contact, when the ridge is in plastic deformation, the total contact stiffness of the conventional hydrodynamic lubricated areas is slightly increased with the reduction of the film thickness H but is positive and small, while the total contact stiffness of the direct contacts between the contact surfaces is constant and reaches a large negative value. When the ridge is in plastic deformation, the contact stiffness of the whole contact is close to the total contact stiffness of the direct contacts between the contact surfaces, only except that it is considerably lower than the total contact stiffness of the direct contacts between the contact surfaces in magnitude when the film thickness H is significantly low.

Load partition in the contact: Figure 13a and b show the ratios R_w of the carried load by the lubricant film lubricated area to that by the whole contact as function of the film thickness H for different values of the half ridge angle θ in the present contact. Figure 13a and b show that for a given value of the half ridge angle θ, when the film thickness H is relatively high, the value of R_w is drastically reduced with the reduction of the film thickness H

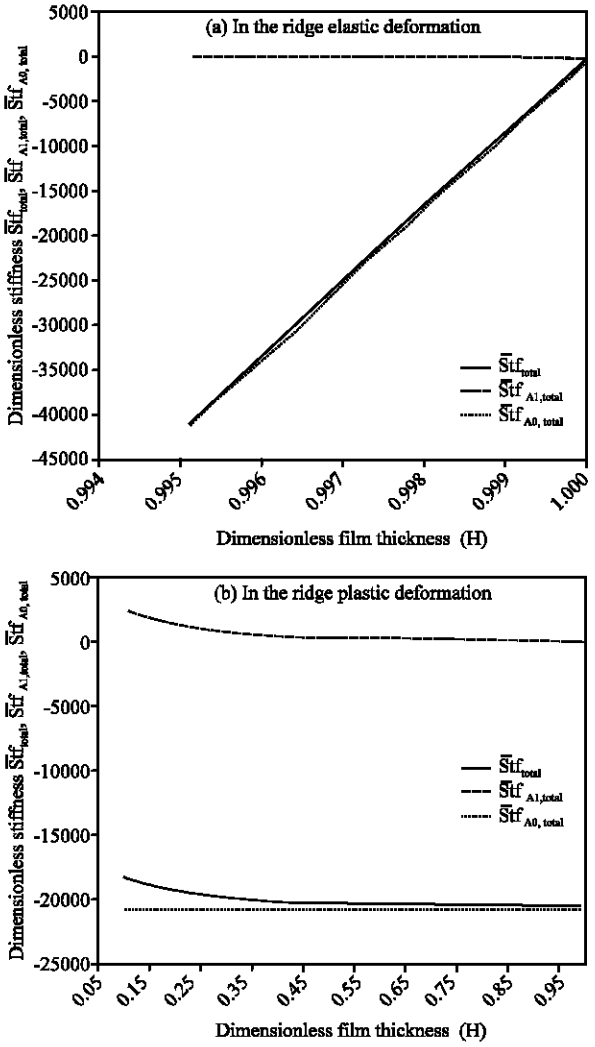

Fig. 12: Total contact stiffness of the whole contact, the conventional hydrodynamic lubricated areas and the direct contacts between the contact surfaces in the present contact as function of the film thickness H when the half ridge angle θ is 25°

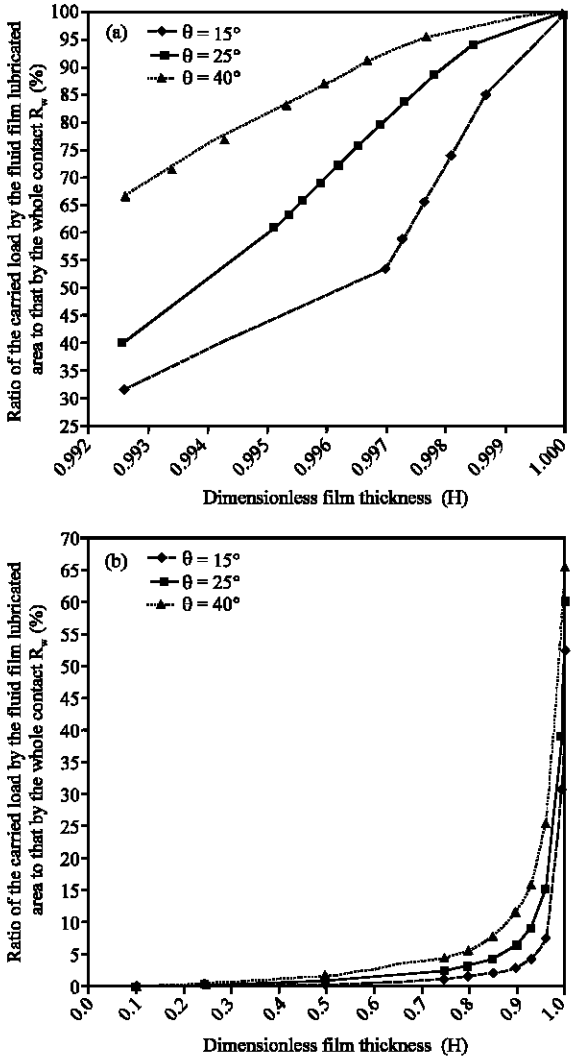

Fig. 13: Ratios R_w of the carried load by the lubricant film lubricated area to that by the whole contact as function of the film thickness H for different values of the half ridge angle θ in the present contact

particularly for smaller θ values. It is reduced to nearly 25% for θ = 40° and H = 0.95. For a given H value, a higher value of the half ridge angle θ gives a higher value of the parameter R_w. These mean that in the present contact, with the reduction of the film thickness H, the contribution of the total load carried by the direct contacts between the contact surfaces to the load carried by the whole contact is drastically increased and becomes dominant even when the film thickness H is relatively high, while in this case the contribution of the lubricant film lubricated areas to the load carried by the whole contact quickly diminishes; A higher value of the half ridge angle θ gives a larger contribution of the lubricant film lubricated areas to the load carried by the whole contact. It is shown that for the investigated cases, when H≤0.75, the value of R_w is no more than 5%. This means that in these cases the direct contacts between the contact surfaces carry almost all the load of the whole contact.

Contact surface temperature rise: Figure 14a shows the temperature rises on the ridge surface in the direct contact between the contact surfaces for light loads carried by the direct contact and different values of the half ridge angle θ in the present contact when the ridge is in elastic deformation. It is shown that in the ridge elastic

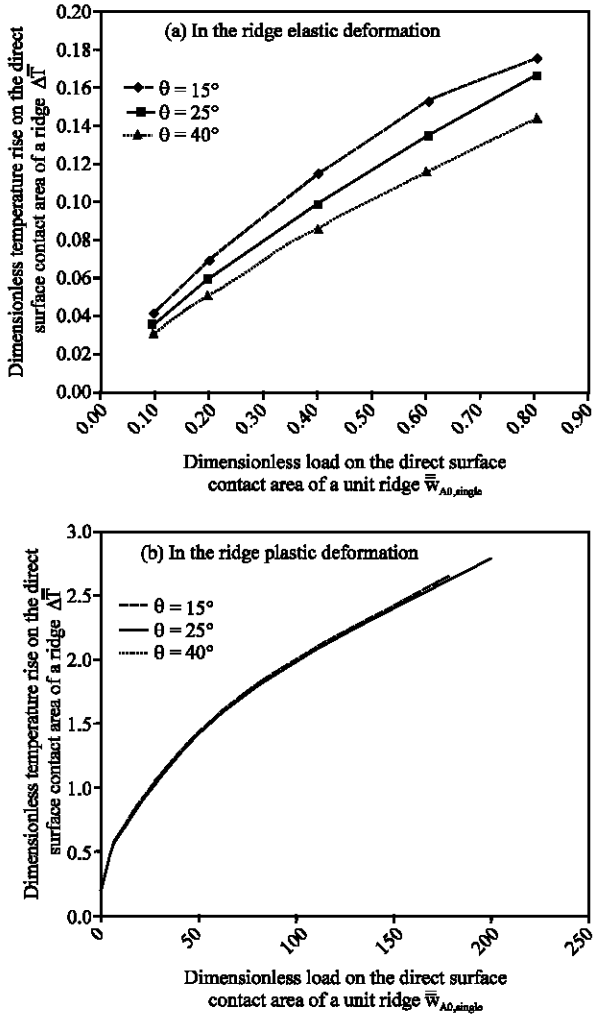

Fig. 14: Temperature rises on the ridge surface in the direct contact between the contact surfaces for different values of the half ridge angle θ in the present contact

deformation regime, for a given value of the half ridge angleθ, the temperature rise on the ridge surface in the direct contact between the contact surfaces is nearly linearly increased with the load carried by the direct contact. It is also shown that in the ridge elastic deformation regime, for the same load carried by the direct contact, there are discrepancies in the temperature rises on the ridge surface in the direct contact between the contact surfaces for different θ values; In the ridge elastic deformation regime, a higher θ value helps to reduce this temperature rise.

Figure 14b shows the temperature rises on the ridge surface in the direct contact between the contact surfaces for relatively heavy loads carried by the direct contact and different values of the half ridge angle θ in the present

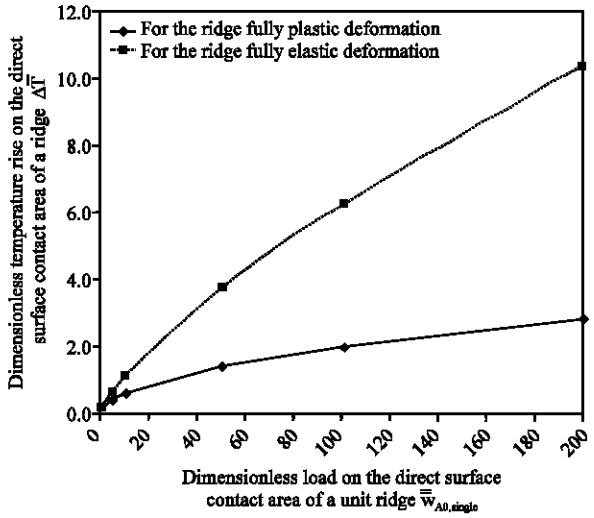

Fig. 14c: Discrepancies of the temperature rises on the ridge surface in the direct contact between the contact surfaces for relatively heavy loads carried by the direct contact when the ridge is, respectively in elastic and plastic deformations and the half ridge angle θ is 25°

contact when the ridge is in plastic deformation. It is theoretically shown that strictly there are no discrepancies in the temperature rises on the ridge surface in the direct contact between the contact surfaces for different θ values for the same load carried by the direct contact when the ridge is in plastic deformation. The minor discrepancies of this temperature rise for different θ values for the same load carried by the direct contact shown in Fig. 14b is due to the computation error. It is shown that in the ridge plastic deformation regime, the temperature rise on the ridge surface in the direct contact between the contact surfaces is considerably increased with the increase of the load carried by the direct contact and is significant for relatively heavy loads carried by the direct contact.

Figure 14c shows the discrepancies of the temperature rises on the ridge surface in the direct contact between the contact surfaces for relatively heavy loads carried by the direct contact when the ridge is, respectively in elastic and plastic deformations and the half ridge angle θ is 25°. It is shown that for the same and heavy load carried by the direct contact, the ridge plastic deformation greatly reduces this temperature rise compared to the ridge elastic deformation result. It means that the ridge plastic deformation helps alleviating the ridge surface temperature rise in the direct contact.

CONCLUSIONS

The present study presents the results obtained from the analysis developed in the first part (Zhang, 2007) for an engineering mixed lubrication contact when the contact surface ridge is isosceles triangle. The modeled contact is one-dimensional composed of a rough plane and another ideally smooth plane. On the rough plane is periodically imposed isosceles triangle ridges. The rough plane is taken as elastic-plastic and moving, while the ideally smooth plane is taken as rigid and stationary. In the modeled contact, the direct contact occurs between the tip of the ridge and the smooth plane, while between other parts of the ridge and the smooth plane, respectively occur the conventional hydrodynamic lubricated contact and the physical adsorbed boundary layer contact according to the lubricating film formed between these mated contact surfaces. The contact regimes of the modeled contact are thus quite mixed. It is more engineering and realistic.

The obtained results in the present study show that in the present contact, when the contact surface ridge is in elastic deformation, with the reduction of the separation between the two planes, the total loads carried by the whole contact and the direct contacts between the contact surfaces both are rapidly increased, while the total load carried by the conventional hydrodynamic lubricated areas nearly remains constant; When the contact surface ridge is in plastic deformation, these two total loads are linearly and rapidly increased with the reduction of the separation between the two planes, while the total load carried by the conventional hydrodynamic lubricated areas is linearly and gradually reduced with the reduction of the separation between the two planes. It is shown that in the ridge plastic deformation regime, the total load carried by the whole contact is mainly contributed by the direct contacts between the contact surfaces, while the contribution of the conventional hydrodynamic lubricated areas to the total load carried by the whole contact is usually negligible. When the ridge is in elastic deformation, a larger value of the half ridge angle θ tends to give a higher load-carrying capacity of the whole contact; While, when the ridge is in plastic deformation, a smaller value of the half ridge angle θ gives a higher load-carrying capacity of the whole contact.

When the ridge is in elastic deformation, the magnitudes of the total contact stiffness of both the whole contact and the direct contacts between the contact surfaces are linearly rapidly increased with the reduction of the separation between the two planes; The contact stiffness of the whole contact is contributed mainly by the total contact stiffness of the direct contacts between the contact surfaces. While, when the ridge is in plastic deformation, the total contact stiffness of the direct contacts between the contact surfaces is constant, reaches a large negative value and is close to the contact stiffness of the whole contact.

With the reduction of the separation between the two planes, the contribution of the total load carried by the direct contacts between the contact surfaces to the load carried by the whole contact is drastically increased and becomes dominant even when the separation between the two planes is relatively high, while in this case the contribution of the lubricant film lubricated areas to the load carried by the whole contact quickly diminishes. A larger value of the half ridge angle θ gives a larger contribution of the lubricant film lubricated areas to the load carried by the whole contact.

When the ridge is in elastic deformation, a higher value of the half ridge angle θ helps to reduce the temperature rise on the ridge surface in the direct contact between the contact surfaces; While, when the ridge is in plastic deformation, the half ridge angle θ has no effect on this temperature rise. The ridge plastic deformation helps alleviating the ridge surface temperature rise in the direct contact.

NOMENCLATURE

a_0, a_1, a_2	=	Parameters appearing in Eq. 1
c_m	=	Specific heat of the rough surface
C_y	=	Function of film thickness, Eq. 1
E_a	=	Young's module of elasticity of the contact surface
f	=	Friction coefficient of the ridge-plane direct contact area
h	=	Film thickness between the root of the ridge and the smooth plane
$h_{cr,e}$	=	(critical) value of the film thickness h when the ridge is in the maximum elastic deformation
$h_{cr,ncf}$	=	Critical thickness of the physical adsorbed layer boundary lubrication film
h_x	=	Lubricant film thickness at a coordinate x
h_0	=	Initial height of the ridge
H	=	Dimensionless film thickness, h/h_0
$H_{cr,e}$	=	$h_{cr,e}/h_0$
k_m	=	Heat conduction coefficient of the rough surface
N	=	Number of the surface ridge in the whole contact
p	=	Dimensional lubricant film pressure
p_y	=	Compressive yielding strength of the ridge
P	=	Dimensionless pressure, αp

r	=	Approaching zero value
R_w	=	Ratio of the carried load by the lubricant film lubricated area to that by the whole contact in the present modeled contact
$\bar{Stf}$	=	Dimensionless stiffness, d $\bar{w}$ /dH
$\bar{\bar{Stf}}$	=	Universally normalized stiffness, d $\bar{\bar{w}}$ /dH
T_a	=	Ambient temperature, 20°C
u	=	Sliding speed between the contact surfaces
w	=	Dimensional load per unit contact length
$w_{max,e}$	=	Maximum load on the direct surface contact area between a single ridge and the smooth plane when the ridge undergoes elastic deformation
$w_{ul,\ total}$	=	Load per unit contact width in the whole contact
$\bar{w}$	=	Dimensionless load, $w/w_{max,e}$
$\bar{\bar{w}}$	=	Universally normalized load, $w/w_{max,e}\big\vert_{\theta=25}$
$\bar{w}_{ul,\ total}$	=	$w_{ul,\ total}\ h_0/w_{max,e}$
$\bar{\bar{w}}_{ul,\ total}$	=	$w_{ul,\ total}\ h_0/w_{max,e}\big\vert_{\theta=25°}$
x	=	Coordinate shown in Fig.1b
X	=	Dimensionless coordinate, x/h_0
v	=	Poisson's ratio of the contact surface
θ	=	Half ridge angle
η_{ncf}^{eff}	=	Effective viscosity of the boundary adhering layer
η_0	=	Viscosity of continuum lubricant at ambient condition
α	=	Viscosity-pressure index of lubricant
ρ_m	=	Density of the rough surface
ΔT	=	Dimensional temperature rise of the direct contact area between the ridge and the smooth plane
$\Delta \bar{T}$	=	Dimensionless temperature rise, $\Delta T/Ta$

SUBSCRIPTS

A_0	=	On the direct surface contact area
A_1	=	In the zone A_1 shown in Fig. 1b
A_2	=	In the zone A_2 shown in Fig. 1b
single	=	Between a single ridge and the smooth plane
total	=	Of the whole contact in the present model
A_0, total	=	Of the total direct surface contact area in the whole contact
A_1, total	=	Of the total conventional hydrodynamic lubricated area in the whole contact

REFERENCES

Zhang, Y.B. and G.S. Lu, 2005. Flow factor for molecularly thin fluid films in one-dimensional flow due to fluid discontinuity. J. Mol. Liq., 116: 43-50.

Zhang, Y.B., 2006a. Boundary lubrication-An important lubrication in the following time. J. Mol. Liq., 128: 56-59.

Zhang, Y.B., 2006b. Contact-fluid interfacial slippage in hydrodynamic lubricated contacts. J. Mol. Liq., 128: 99-104.

Zhang, Y.B., 2006c. Flow factor of non-continuum fluids in one-dimensional contact. Industr. Lubri. Trib., 58: 151-169.

Zhang, Y.B., 2006d. Flow factor approach to molecularly thin hydrodynamic film lubrication. J. Mol. Liq., 128: 60-64.

Zhang, Y.B., 2007. Study of an engineering mixed contact: Part I- Theoretical analysis. J. Applied Sci., (Paper in Press).